Catalysis Science & Technology

PAPER

View Article Online
View Journal

Cite this: DOI: 10.1039/c4cy00688g

Transition metal-rich mesoporous silicas and their enhanced catalytic properties†

Baowang Lu* and Katsuya Kawamoto

A controllable and simple direct hydrothermal synthesis route was designed for synthesizing well-ordered mesoporous silica incorporating transition metals (M) (Ni, Cu, Zn, Co) with high metal loading. M-incorporated mesoporous silica could be obtained from a starting synthesis mixture with a Si/M mole ratio of 5 using transition metal–ammonia (NH_3) complex ions $[M(NH_3)_x]^{n+}$ as base. The Si/M mole ratio of 5 is the lowest value yet reported. XPS, UV-vis and H_2-TPR analyses demonstrated that a chemical bond was formed between metal and silicon *via* oxygen and no bulk metal oxides existed in any of the M-MCM-41 samples; in other words, only tetrahedral coordinated metal species were detected. The formation of –O–M–O–Si–O– is completed *via* the reaction between hydrolyzate $[M(OH)(NH_3)_{x-1}]^{(n-1)+}$ from $[M(NH_3)_x]^{n+}$ and ≡Si–OH (silanol sites) from a silica source (tetramethoxysilane (TMOS)). All the M-MCM-41 samples possessed remarkable physical properties and thermal stability. Ni-MCM-41, Cu-MCM-41 and CoMCM-41 catalysts exhibited excellent catalytic efficiency for carbon dioxide (CO_2) hydrogenation, although Zn-MCM-41 catalyst did not. Ni-MCM-41 catalyst suited methanation, resulting in high CO_2 conversion rate and methane selectivity, while Cu-MCM-41 catalyst favored the reverse water gas shift (RWGS) reaction and realized high CO_2 conversion rate to carbon monoxide. A kinetic study was also carried out for methanation and RWGS reaction. Using Ni-MCM-41 catalyst for methanation, the rate equation could be expressed as $r = kC_{CO_2}{}^{0.68}C_{H_2}{}^{3.31}$, where C represents concentration. Using Cu-MCM-41 catalyst for RWGS reaction, the rate equation could be expressed as $r = kC_{CO_2}{}^{0.5}C_{H_2}{}^{1.1}$, where C represents concentration.

Received 28th May 2014,
Accepted 22nd July 2014

DOI: 10.1039/c4cy00688g

www.rsc.org/catalysis

1. Introduction

The discovery of mesoporous molecular sieves (MMS) as catalysts or catalyst supports has opened a new research area. Ordered MMS are not often used as catalysts. Much more frequently, transition metals are introduced to add their catalytic functions. Transition metals can be introduced into MMS either from the synthesis mixture during MMS synthesis using a direct synthesis method[1–4] or by post-synthesis modification,[5–15] and the high loading of the transition metal is also always desirable. Because an excessive amount of transition metal in the synthesis mixture may hinder the development of a particular mesoporous structure,[4] impregnation, which is a commonly used post-synthesis method, is the only way to introduce the maximum amount of transition metal.[3] However, metal nanoparticles generated on MMS by the post-synthesis method typically lack uniformity as regards size and shape due to particle aggregates and exhibit low catalytic activity owing to low dispersion. To take advantage of MMS materials incorporating transition metals as catalysts, we must develop an extremely effective transition metal incorporation method. Much effort has been focused on the incorporation of transition metal;[16–18] however, the incorporated amount has been limited to less than 5.5 wt% (Si/Ni = 16.6).[16]

Here, we report a controllable and simple direct hydrothermal synthesis route for incorporating a transition metal (M = nickel (Ni), copper (Cu), zinc (Zn), cobalt (Co)) into mesoporous silica with a large amount (Si/M = 5). The catalytic properties were further investigated using carbon dioxide (CO_2) hydrogenation.

2. Experimental

2.1. Synthesis of transition metal-incorporated mesoporous silica

The synthesis of transition metal-rich mesoporous silica was carried out as follows.

(1) Transition metal (M)–ammonia (NH_3) complex ions were prepared using different $M(NO_3)_x$ (nickel(II) nitrate hexahydrate, $Ni(NO_3)_2{\cdot}6H_2O$, 98%, Wako, Japan; copper(II) nitrate 3-hydrate, $Cu(NO_3)_2{\cdot}3H_2O$, 99.5%, Kishida, Japan; cobalt(II) nitrate hexahydrate, $Co(NO_3)_2{\cdot}6H_2O$, 98%, Wako, Japan; zinc(II)

Graduate School of Environmental and Life Science, Okayama University, 3-1-1 Tsushima-naka, Kita-ku, Okayama-shi, Okayama, 700-8530, Japan. E-mail: baowanglu@okayama-u.ac.jp; Tel: +81 86 2518842

† Electronic supplementary information (ESI) available. See DOI: 10.1039/c4cy00688g

nitrate hexahydrate, $Zn(NO_3)_2{\cdot}6H_2O$, 99%, Kishida, Japan) and NH_3 solutions (28–30.0%, Kishida, Japan).

(2) 3.52 g of surfactant (hexadecyltrimethylammonium bromide, cetyltrimethyl ammonium bromide, C_{16}TMABr, Wako, Japan) was dissolved in 400 g of water and 400 g of methanol (CH_3OH, MeOH, 99.7%, Wako, Japan), and then 4.62 g of tetramethyl orthosilicate (tetramethoxysiliane, TMOS, 99.7%, Tokyo Chemical Industry Co., Ltd., Japan) was added at room temperature. After stirring for 30 min, the above transition metal–ammonia complex ions were added and then aged under stirring for 24 h. The white solid product obtained was filtered, washed thoroughly with deionized water, dried overnight at room temperature, and calcined at 550 °C for 10 h.

2.2. Characterization

The X-ray diffraction (XRD) patterns of the solid products were collected using a powder X-ray diffractometer (Rigaku Multiflex) with graphite monochromatized Cu Kα radiation at 40 kV and 26 mA. Nitrogen (N_2) adsorption isotherms at −196 °C were obtained using a conventional volumetric apparatus (Quadrasorb USA). Before the adsorption measurements were made, the powders (≈0.1 g) were subjected to a temperature of 300 °C for 5 h in a vacuum. The specific surface area was calculated with the Brunauer–Emmett–Teller (BET) method. The pore size was calculated from the desorption branch of nitrogen adsorption–desorption isotherms by the Barrett–Joyner–Halenda (BJH) method. The pore volume was taken at a single point P/P_0 = 0.95. The morphology was observed with a scanning electron microscope (SEM, JEOL JSM-7600F). The solid product was observed using a transmission electron microscope (TEM, JEOL JEM-2100) at an electron acceleration of 200 kV. X-ray photoelectron spectroscopic (XPS) experiments were performed with a ULVAC-PHI, Inc. Qantera XPS/AES system. Sample charging was accounted for using the C 1s peak of adventitious hydrocarbon surface contamination. UV-vis diffuse reflectance spectra (UV-vis DRS) were recorded in the range of 200–800 nm on a PerkinElmer LAMBDA 950 spectrophotometer. The bulk chemical compositions were measured by using an inductively coupled plasma-optical emission spectrometer (ICP-OES, Thermo Scientific, iCAP 6000 series).

Catalyst reducibility was also studied by temperature-programmed reduction (TPR) in a BET-CAT Catalyst Analyzer (BEL Japan Inc.) using hydrogen (H_2). The samples were pretreated for 1 h at 500 °C in synthetic air (25 ml min^{-1}) followed by cooling to 50 °C in a pure argon (Ar) stream (25 ml min^{-1}). After switching to 10 vol.% H_2 in Ar (total flow rate: 25 ml min^{-1}), the temperature was increased linearly at a rate of 5 °C min^{-1} from 50 °C to 900 °C. All TPR data were normalized to the respective sample weight and expressed in arbitrary units.

2.3. Catalytic reaction

The catalysts were pre-reduced *in situ* in a H_2/N_2 stream for 2 h at a heating ramp rate of 1 °C min^{-1}. The reaction was performed at atmospheric pressure in a fixed-bed quartz reactor with a 20 mm inside diameter. A 30 mm long catalyst (2 g) between two layers of quartz wool was loaded into the reactor. A thermocouple was inserted directly into the center of the catalyst bed to measure the actual pretreatment and reaction temperatures *in situ*. The reactor was heated in a furnace (KTF-035N, Koyo Thermo Systems, Co., Ltd.) equipped with a temperature controller. All reactant gases were monitored with a mass flow meter (E-40) and a controller (PE-D20) (HORIBA STEC, Co., Ltd.). The flow of the product was measured with a film flow meter (VP-3, HORIBA STEC, Co., Ltd.) and analyzed with a gas chromatography-thermal conductivity detector (GC-TCD) after the reaction had become stable.

3. Results and discussion

3.1 Synthesis of transition metal-incorporated mesoporous silica

M-incorporated mesoporous silica was successfully obtained from a starting synthesis mixture with a Si/M mole ratio of 5 by modifying Stöber's procedure[19] with the addition of cetyltrimethyl ammonium bromide (C_{16}TMABr) as a template, using a water (H_2O)–methanol (MeOH) system, in the presence of transition metal (M)–ammonia (NH_3) complex ions $[M(NH_3)_x]^{n+}$ as base, through the hydrolysis of tetramethoxysilane (TMOS) and the condensation of silica species, under appropriate synthesis conditions (as shown in Table 1). We also describe the procedure in more detail in the ESI.† As shown in Fig. 1(A), all the samples were characterized by XRD as having the typical hexagonal structure of MCM-41.[20] Well-ordered two-dimensional hexagonal structures were observed regardless of the incorporation of transition metals, which gave a sharp (100) plane diffraction peak and the diffraction peaks of higher Miller index planes of (110) and (200) (inserted XRD pattern). No peaks assigned to oxides were confirmed; however, peaks originating from M-containing phyllosilicates[21] were observed (inserted XRD pattern), suggesting that all the transition metals were incorporated into the MCM-41 structure and existed as M-containing phyllosilicates or as oxides with a very small size. In addition, after undertaking a detailed investigation of the existence of M-containing phyllosilicates in M-MCM-41 with various Si/M mole ratios by XRD, we found that they decreased with increasing Si/M ratio and disappeared when the Si/M mole ratio reached 20. The nitrogen adsorption/desorption isotherms are shown in Fig. 1(B). The isotherms were typical for MCM-41 (ref. 20) and similar to the type IV IUPAC classification,[22] clearly indicating that these materials possessed mesoporous structures. In addition, a type-H1 hysteresis loop was observed in the nitrogen adsorption/desorption isotherms. All the samples exhibited a sharp capillary condensation step in the adsorption isotherms, indicating that highly ordered MCM-41 was obtained even when a large amount of transition metal was incorporated. From our knowledge of the direct synthesis of M (Ni, Cu, Zn, CO)-MCM-41, the Si/M mole ratio of 5 is the lowest value yet reported. We also tried

Table 1 Synthesis and characteristics of various M-MCM-41 samples

Sample	Starting gel[a]		Product[b]						
			Si/M						
	NH_3/M	Si/M	ICP	TPR	d_{100} (nm)	S_{BET} (m^2 g^{-1})	PV (cm^3 g^{-1})	PD (nm)	*WT* (nm)
Ni(5)-MCM-41	7	5	5.42	5.64	3.53	962	0.50	2.18	1.90
Cu(5)-MCM-41	7	5	4.68	4.59	3.63	623	0.36	2.18	2.01
Zn(5)-MCM-41	6	5	5.32	—	3.53	789	0.31	1.91	2.17
Co(5)-MCM-41	30	5	5.21	6.46	3.18	631	0.43	2.20	1.47

[a] Synthesis conditions: MeOH/(MeOH + H_2O) = 50 wt%, C_{16}TMABr/TMOS = 0.32, TEOS/(MeOH + H_2O) = 3.79×10^{-5}. [b] S_{BET}: surface area (calculated by using the Brunauer–Emmett–Teller (BET) method in the relative pressure range of p/p_0 = 0.05–0.3); PV: pore volume (obtained from the volumes of N_2 adsorbed at p/p_0 = 0.95 or in the vicinity); PD: pore diameter (analyzed by the desorption branch of the isotherms by the Barrett–Joyner–Halenda (BJH) method) and *W*: wall thicknesses (calculated by $(2 \times d_{100}/\sqrt{3})$ – pore size).

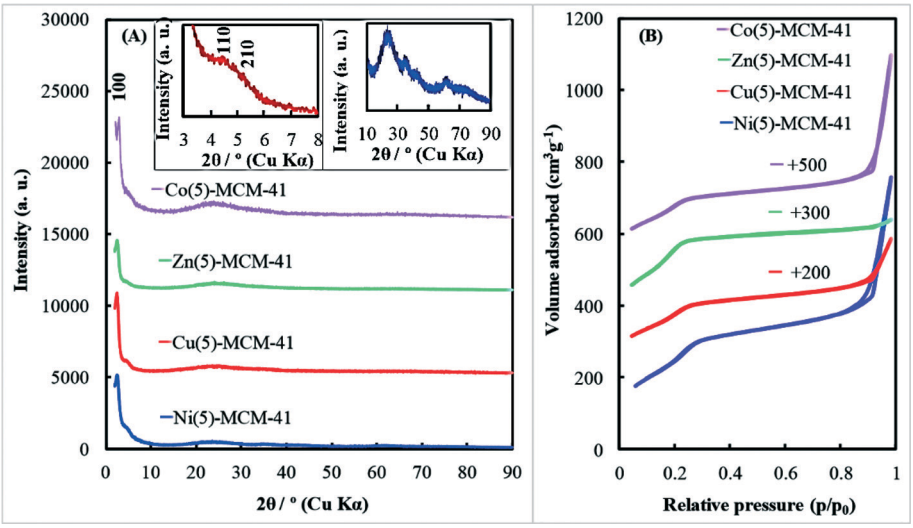

Fig. 1 XRD patterns (A) and nitrogen adsorption/desorption isotherms (B) of various MMCM-41 samples obtained from a starting synthesis mixture with a Si/M mole ratio of 5.

to synthesize M-MCM-41 using a starting synthesis mixture with a lower Si/M mole ratio, and the nitrogen adsorption/desorption isotherms of products obtained from the starting synthesis mixture with the Si/M mole ratios of 3 and 4 were typical for MCM-41 (ref. 20) and similar to the type IV IUPAC classification.[22] Unfortunately, the diffraction peaks assigned to mesoporous materials could not be observed, clearly indicating that these materials obtained from the starting synthesis mixture with the Si/M mole ratios of 3 and 4 had disordered mesoporous structures. However, metal oxides could not still be confirmed in products obtained from the starting synthesis mixture with the Si/M mole ratios of 3 and 4.

Table 1 also shows the chemical and physical characteristics of various M-MCM-41 samples obtained from the starting synthesis mixture with the Si/M mole ratio of 5. There was a slight difference between the Si/M ratios of the starting gel and the product. All the M-MCM-41 samples exhibited a high special surface area, a large pore volume and a large pore size, similar to mesoporous pure silica.[23] All the materials had a typical wall thickness for MCM-41.[20] SEM images (Fig. S1†) show that all M-MCM-41 samples had both a spherical morphology and irregular aggregates. TEM images (Fig. S2†) show that all the M-MCM-41 samples had the highly ordered hexagonal structure of MCM-41.

The chemical nature, such as the chemical and coordinate states of the transition metal in M-MCM-41 obtained from a starting synthesis mixture with a Si/M mole ratio of 5, was further studied by XPS and UV-vis spectroscopy. The M $2p_{3/2}$, O 1s and Si 2p XPS spectra are shown in Fig. 2. The measured binding energies are summarized in Table 2. To the best of our knowledge, there is still no relevant information available on the M $2p_{3/2}$, O 1s and Si 2p XPS spectra of M (Ni, Cu, Zn, Co)-MCM-41. Therefore, for comparison, the $2p_{3/2}$ and O 1s binding energies of various potentially pertinent oxides along with pure silica MCM-41 are also shown in Table 2. Because there was no obvious difference among the Si 2p binding energies of M-MCM-41, SiO_2 and pure silica MCM-41, it appears that the Si 2p binding energy was not particularly helpful for the chemical identification of the local environment of the metal. All the M $2p_{3/2}$ and O 1s binding energies of M-MCM-41 samples were distinctly higher than those of metal oxides, indicating that there was a strong interaction between metal and silicon. In addition, with respect to the information in Table 2, we found that the Ni $2p_{3/2}$ and O 1s

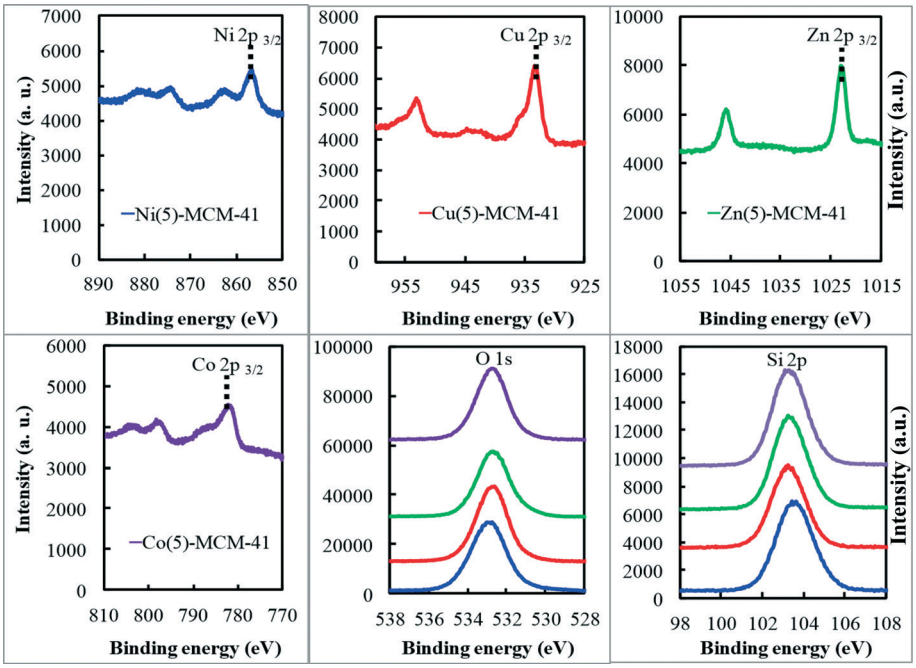

Fig. 2 M $2p_{3/2}$, O 1s and Si 2p XPS spectra of various M-MCM-41 samples obtained from a starting synthesis mixture with a Si/M mole ratio of 5 (–Ni(5)-MCM-41, –Cu(5)-MCM-41, –Zn(5)-MCM-41, and –Co(5)-MCM-41).

Table 2 Binding energies of reference oxides and various M-MCM-41 samples

Compound	M $2p_{3/2}$ (eV)		O 1s (eV)	Si 2p (eV)	Reference
	M	$2p_{3/2}$ (eV)			
NiO	Ni	854.0–854.9	529.6–530.4	—	24–33
SiO_2	—	—	532.2–533.1	103.2–103.7	26, 27, 31 and 33
CuO	Cu	932.3	529–531	—	34, 35
ZnO	Zn	1021.3–1021.6	530.2–530.5	—	36, 37
Co_3O_4	Co	779.6–780.1	529.5–531.4	—	38–40
2 : 1 Ni phyllosilicate	Ni	856.9–857.0	532.1–532.5	103.1–103.3	29, 33
Ni(5)-MCM-41	Ni	856.7	532.75	103.45	This study
Cu(5)-MCM-41	Cu	933.4	532.65	103.3	This study
Zn(5)-MCM-41	Zn	1023	532.75	103.25	This study
Co(5)-MCM-41	Co	782.2	532.6	103.1	This study
MCM-41	—	—	532.66	103.25	This study

binding energies of Ni-MCM-41 samples were similar to those of 2 : 1 Ni phyllosilicates.[29,33] Therefore, no contributions originating from metal oxides in M-MCM-41 samples were apparent; in other words, all the metals were incorporated into the MCM-41 structure or existed as M-containing phyllosilicates (in particular, 2 : 1 phyllosilicates), which have higher M $2p_{3/2}$ binding energies than metal oxides. These results strongly support those obtained with XRD. Although both M-MCM-41 and MCM-41 exhibit similar O 1s binding energy, two deconvoluted peaks were observed in the O 1s spectrum of the M-CM-41 sample (not shown here), which were assigned to two oxygen species bonded to silicon in pure silica MCM-41 and metal, respectively, and the peak at higher binding energy can be assigned to the oxygen bonded to metal.[41] Therefore, M $2p_{3/2}$ and O 1s binding energies can be used to study the local environment of metals.

Fig. 3 shows the UV-vis spectra of various M-MCM-41 samples. As far as we know, there is still no relevant information available on the UV-vis spectra of M (Ni, Cu, Zn, Co)-MCM-41. Therefore, after a careful comparison with results reported in the literature,[42–48] metal oxide absorption bands were not observed, indicating that all the metals were incorporated into the MCM-41 structure or existed as M-containing phyllosilicates, and this confirmed our above results obtained with XRD and XPS. It was noted that all the absorption bands of the metal were shifted to lower wavelengths compared with those of the bulk metal oxides, indicating the formation of –O–M–O–Si–O–, namely, a chemical bond was formed between silicon and metal *via* oxygen. Therefore, all metal species in the M-MCM-41 sample existed in tetrahedral coordination. For example, in the Co-MCM-41 UV-vis spectrum, three well-defined absorption bands were observed at 527, 594 and

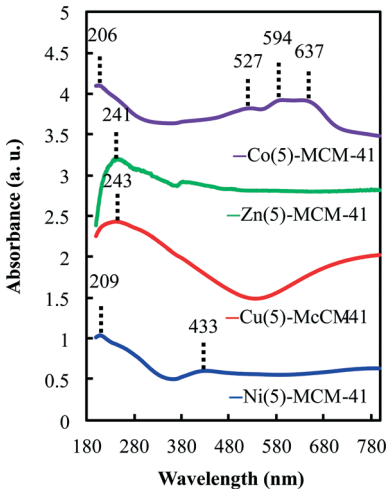

Fig. 3 UV-vis absorbance spectra of various M-MCM-41 samples obtained from a starting synthesis mixture with a Si/M mole ratio of 5.

635 nm, indicating the presence of Co species in tetrahedral coordination and there was no evidence at 480 nm that could be attributed to octahedral coordination Co species.[49]

TPR investigation is generally useful as a fingerprint of a metal species' interaction with the support material. As shown in Fig. 4, for the Ni-MCM-41 sample, H_2-TPR profiles exhibited a single broad peak centered at 651 °C, which was higher than that of NiO-supported SBA-15,[50] indicating that to reduce Ni ions, Si–O–Ni bond cleavage is required.[51] For the Co-MCM-41 sample, two peaks appeared around 725 and 820 °C assigned to the stepwise reduction of Co_2O_3,[52] which were higher than the reduced temperature of Co_2O_3.[52] For the Zn-MCM-41 sample, two peaks appeared around relatively high temperatures of 843 and 882 °C. For the Cu-MCM-41 sample, a sharp peak around 242 °C could be observed, although this temperature was the lowest among these M-MCM-41 samples, which was higher than that of CuO supported.[53] Therefore, we can conclude that in all M-MCM-41 samples, the metals were incorporated into the MCM-41 structure from TPR studies. In addition, the Si/M ratios were also calculated by TPR and given in Table 1. There is no large difference in the Si/M ratio obtained between ICP and TPR.

Because transition metal–ammonia complex ions $[M(Ni, Cu, Zn, Co)(NH_3)_x]^{n+}$ are highly soluble even in basic medium, metal hydroxides are formed with difficulty, with the result that no oxides had formed after calcination. Then, the formation mechanism of transition metal-incorporated mesoporous silica was considered and is shown in Fig. 5. $[M(NH_3)_x]^{n+}$ first hydrolyzes with H_2O to form $[M(OH)(NH_3)_{x-1}]^{(n-1)+}$ and is then adsorbed at the surface of silanol sites (≡Si–OH) derived from the hydrolysis of silica source TMOS. The formation of –O–M–O–Si–O– is completed *via* the reaction between $[M(OH)(NH_3)_{x-1}]^{(n-1)+}$ and ≡Si–OH.

Even with calcination at 700 °C, no metal oxides were observed in the XRD pattern of the M-MCM-41 sample obtained from a starting synthesis mixture with a Si/M mole ratio of 5, indicating that there was high thermal stability

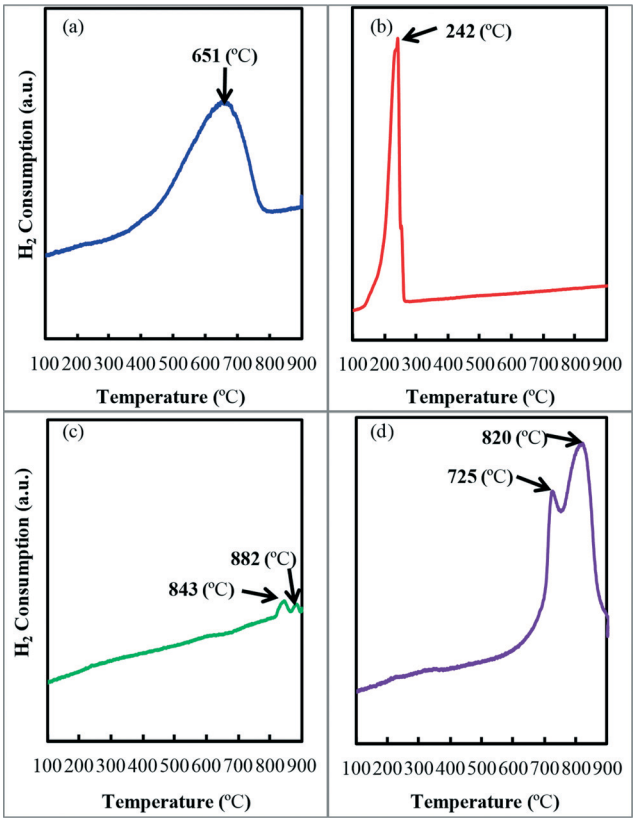

Fig. 4 H_2-TPR profiles of various M-MCM-41 samples obtained from a starting synthesis mixture with a Si/M mole ratio of 5. (a) Ni-MCM-41, (b) Cu-NCM-41, (c) Zn-MCM-41, and (d) Co-MCM-41.

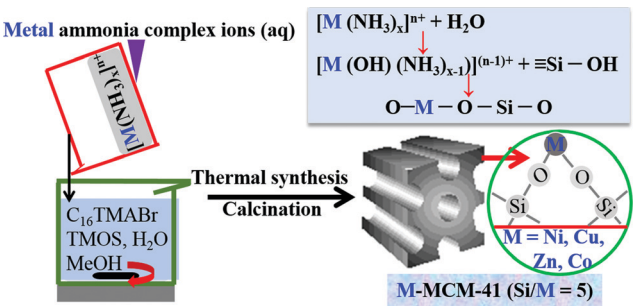

Fig. 5 Formation mechanism of transition metal-incorporated mesoporous silica.

even with a low Si/M ratio of 5. Therefore, the M-MCM-41 sample obtained from a starting synthesis mixture with a Si/M mole ratio of 5 can be expected to provide a highly effective catalyst that can operate at high temperatures.

3.2. Catalytic reaction

CO_2 hydrogenation was carried out to evaluate the catalytic performance of various M-MCM-41 samples obtained from the starting synthesis mixture with the Si/M mole ratio of 5. Fig. 6 shows the results of CO_2 hydrogenation using various M-MCM-41 catalysts. The turnover frequencies (TOFs) and

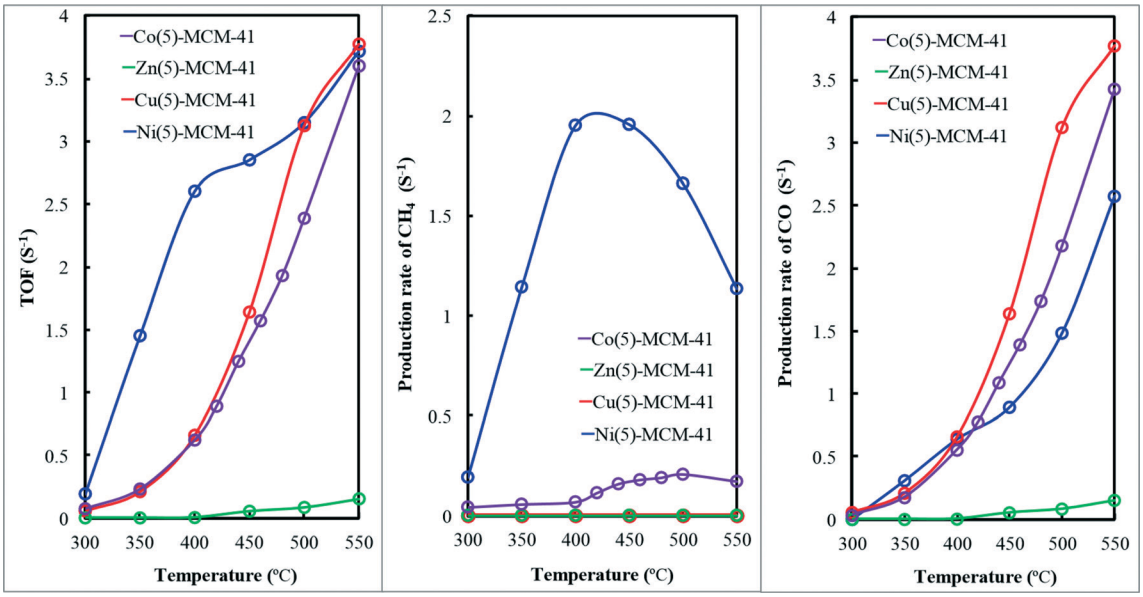

Fig. 6 TOFs and production rates of CH_4 and CO obtained using various M-MCM-41 catalysts obtained from a starting synthesis mixture with a Si/M mole ratio of 5. Reduction conditions: temperature 550 °C (heating rate: 1 °C min^{-1}), gas flow $H_2 : N_2$ = 120 : 30 ml min^{-1}, time 2 h. Catalyst reaction conditions: gas flow $H_2 : CO_2$ = 120 : 120 ml min^{-1}.

the rates of CO and CH_4 production were calculated by CO_2 conversion and CO and CH_4 production divided by the total amount of metal oxide used. Regardless of the presence of M-CM-41 catalysts, the CO_2 conversion rate increased with increasing temperature. When Zn-MCM-41 catalyst was used, almost no CO_2 conversion occurred. The order of CO_2 conversion rate obtained using different M-MCM-41 catalysts was Ni-MCM-41 > Cu-MCM-41 ≈ Co-MCM-41 ≫ Zn-MCM-41. According to the mechanism of CO_2 hydrogenation, the dissociation of H_2 adsorbed to H atom and CO_2 adsorption are two important steps occurring on the metal atom surface, and H_2 dissociation is a key step. Ni atom favors H_2 dissociation to H, while Cu atom does not (just suits CO_2 adsorption), resulting in Ni-MCM-41 giving higher CO_2 conversion than Cu-MCM-41. The reduction of a Co ion to a Co atom needs a higher temperature compared to the reduction of a Ni ion, which provides a smaller amount of Co atom, so Co-MCM-41 exhibits lower CO_2 conversion than Ni-MCM-41. Because almost no Zn atom was derived from the reduction of Zn ion, no CO_2 hydrogenation occurs on Zn-MCM-41. However, it seems that there is no obvious difference in the CO_2 conversion of Ni-MCM41, Cu-MCM-41 and Co-MCM-41 catalysts at 550 °C. When Ni-MCM-41 catalyst was used, methanation occurred as the main reaction along with the reverse water gas shift (RWGS) reaction as a by-reaction, while in the presence of Co-MCM-41 as a catalyst, methanation was a by-reaction and the RWGS reaction was the main reaction. Therefore, the methane (CH_4) production rate obtained using Ni-MCM-41 catalyst was far higher than that obtained using Co-MCM-41 catalyst, while the order of carbon monoxide (CO) production rate realized using two catalysts was exactly opposite to that of the CH_4 production rate. When Cu-MCM-41 and Zn-MCM-41 catalysts were employed, only the RWGS reaction occurred, although their CO selectivity was close to 100% and the CO production rate using Cu-MCM-41 was much greater than that using Zn-MCM-41 catalyst. The above CO_2 hydrogenation result indicates that Ni-MCM-41 catalyst favors methanation owing to its high CO_2 conversion rate and CH_4 selectivity, while Cu-MCM-41 catalyst was advantageous for the RWGS reaction due to its high CO_2 conversion rate and close to 100% selectivity. Fig. 7 shows Arrhenius plots calculated for CO_2 conversion using Ni-MCM-41, Cu-MCM-41 and Co-MCM-41 catalysts. The activation energies obtained using various M-MCM-41 catalysts for CO_2 hydrogenation are summarized in Table 3. The activation energy obtained using Ni-MCM-41 catalyst was ≈10 kJ mol^{-1}, while that obtained using Cu-MCM-41 catalyst (≈75 kJ mol^{-1}) was nearly as large as that using Co-MCM-41 catalyst (≈67 kJ mol^{-1}), which was about seven times that using Ni-MCM-41 catalyst. Therefore, the catalytic activity of Ni-MCM-41 catalyst for CO_2 hydrogenation was far higher than those of Cu-MCM-41 and Co-MCM-41 catalysts.

Next, methanation using Ni-MCM-41 catalyst obtained from a starting synthesis mixture with a Si/Ni mole ratio of 5 and RWGS reactions using Cu-MCM-41 catalyst obtained from a starting synthesis mixture with a Si/Cu mole ratio of 5 were further investigated. The results are given in Fig. 8. Fig. 8(A) shows CO_2 conversion rate and CH_4 and CO production rates at different temperatures. Using Ni-MCM-41 as a catalyst for CO_2 methanation, the maximum CO_2 conversion rate was ≈8 S^{-1} (CO_2 conversion of ≈70%). In previous studies,[12,18] when Ni-MCM-51 catalyst with 5 wt% Ni was used, the maximum CO_2 conversion was ≈13%. Therefore, the amount of Ni in Ni-MCM-41 catalyst had a significantly enhanced CO_2 conversion rate. Using Ni-MCM-41 catalyst, the maximum CH_4 yield was 59%, and the CH_4 selectivity was as high as

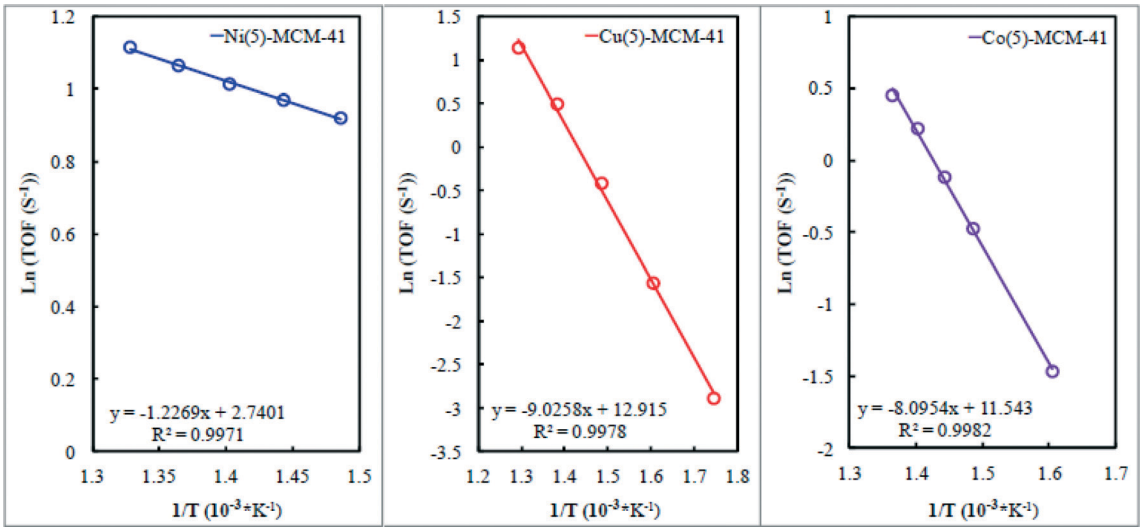

Fig. 7 Arrhenius plots at different temperatures using Ni-MCM-41, Cu-NCM-41, and Co-MCM-41 catalysts obtained from a starting synthesis mixture with a Si/M mole ratio of 5. Reduction conditions: temperature 550 °C (heating rate: 1 °C min^{-1}), gas flow H_2 : N_2 = 120 : 30 ml min^{-1}, time 2 h. Catalyst reaction conditions: gas flow H_2 : CO_2 = 120 : 120 ml min^{-1}.

Table 3 Rate equations and activation energies obtained using various catalysts

Catalyst	Rate equations		Activation energies (kJ mol^{-1})		
	For MN[a]	For RWGS[b]	For MN	For RWGS	Reference
Ni(5)-MCM-41	$r = kC_{CO_2}{}^{0.68}C_{H_2}{}^{3.31}$	—	73.1	10.2	This study
Cu(5)-MCM-41	—	$r = kC_{CO_2}{}^{0.5}C_{H_2}{}^{1.1}$	—	75.3,[c] 60.5[d]	This study
Co(5)-MCM-41	—	—	—	67.6	This study
Ni	$r = kC_{CO_2}{}^{0.5}$	—	85.7	—	54 and 55
Cu/ZnO	—	—	—	138–171	57
NiO/SBA-15	—	$r = kC_{CO_2}{}^{0.5}C_{H_2}{}^{1.1}$	—	—	58
Ni/Al_2O_3		$r = kC_{CO_2}{}^{0.5}C_{H_2}{}^{0.81}$	—	20.8	59

[a] MN: methanation. [b] RWGS: reverse water gas shift reaction. [c] Obtained at reaction temperature of 300–550 °C. [d] Obtained at reaction temperature of 300–600 °C.

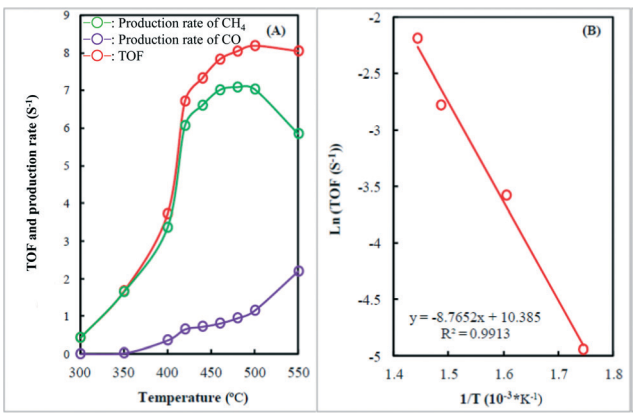

Fig. 8 (A) TOFs and production rates of CH_4 and CO obtained using Ni-MCM-41 catalyst obtained from a starting synthesis mixture with a Si/Ni mole ratio of 5. (B) Arrhenius plots at different temperatures using Ni-MCM-41 catalyst. Catalyst reduction conditions: temperature 550 °C (heating rate: 1 °C min^{-1}), gas flow H_2 : N_2 = 120 : 30 ml min^{-1}, time 2 h. Reaction conditions: gas flow H_2 : CO_2 = 120 : 30 ml min^{-1}.

90%. Fig. 8(B) shows Arrhenius plots calculated for CO_2 methanation using Ni-MCM-41 catalyst. The activation energy obtained using Ni-MCM-41 catalyst for CO_2 methanation was ≈73 kJ mol^{-1}, lower than that reported previously,[54,55] suggesting that Ni-MCM-41 catalyst had high catalytic activity. To obtain kinetic data for CO_2 methanation, the investigation was carried out by varying the CO_2 and H_2 concentrations at 480 °C using Ni-MCM-41 catalyst. The CO_2 reaction order was 0.68, and the H_2 reaction order was 3.31. The rate equation could be expressed as follows: $r = kC_{CO_2}{}^{0.68}C_{H_2}{}^{3.31}$, where C represents concentration, similar to the previous research.[54,55] Therefore, the influence of H_2 concentration was greater than that of CO_2 concentration on CO_2 conversion through methanation, indicating that high H_2 concentration favors CO_2 conversion to methane. After methanation, there is a slight difference in the surface area of the Ni-MCM-41 catalyst between before and after methanation, indicating that it had relatively high thermal stability for methanation.

CO_2 conversion rate to CO and Arrhenius plots calculated from CO_2 conversion to CO using Cu-MCM-41 catalyst through RWGS reactions is shown in Fig. 9. The CO_2 conversion rate to CO increased with increasing temperature, similar to our previous research.[56] The CO_2 conversion rate was as high as ≈5 S^{-1} (CO_2 conversion of ≈40%) even at 600 °C and far higher than that obtained at the same temperature using NiO/SBA15,[56]

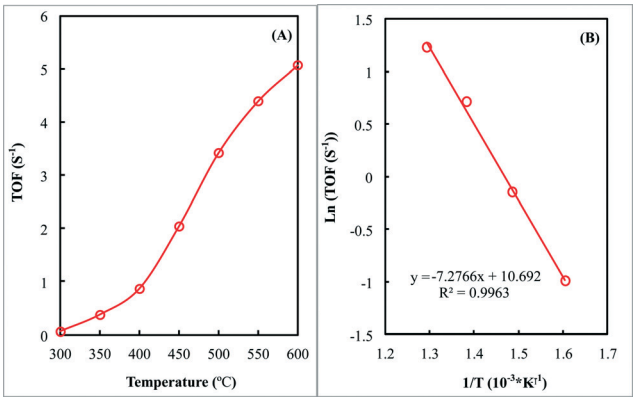

Fig. 9 (A) TOF obtained using Cu-MCM-41 catalyst obtained from a starting synthesis mixture with a Si/Cu mole ratio of 5. (B) Arrhenius plots at different temperatures using Cu-MCM-41 catalyst. Catalyst reduction conditions: temperature 600 °C (heating rate: 1 °C min^{-1}), gas flow H_2 : N_2 = 120 : 30 ml min^{-1}, time 2 h. Reaction conditions: gas flow H_2 : CO_2 = 120 : 120 ml min^{-1}.

which should perform better than copper.[57] The activation energy obtained using Cu-MCM-41 for CO_2 conversion to CO through RWGS reaction was ≈60 kJ mol^{-1}, lower than that reported previously,[58] suggesting that Cu-MCM-41 catalyst had high catalytic activity. To obtain kinetic data for CO_2 conversion to CO through RWGS reaction, the investigation was carried out by varying the CO_2 and H_2 concentrations at 600 °C using Cu-MCM-41 catalyst. The CO_2 reaction order was 0.5, and the H_2 reaction order was 1.1. The rate equation could be expressed as follows: $r = kC_{CO_2}{}^{0.5}C_{H_2}{}^{1.1}$, where C represents concentration, similar to the previous research.[58,59]

Korose–Nowak criterion test. In order to establish that the measured catalytic activity is independent of the influence of transport phenomena,[60] the Korose–Nowak (KN)[61] criterion test modified by Madon–Boudart[62] has been employed. In the present study, the Korose–Nowak test has been performed with Ni-MCM-41 pellet catalysts with different Si/Ni mole ratios for CO_2 methanation. Fig. 10 displays the Koros–Nowak criterion plot of TOF (S^{-1}) *vs.* Si/Ni for CO_2 methanation using Ni-MCM-41 catalyst at 480 °C. The value of the KN number (slope) was found to be 0.996 at 480 °C. The KN number close to unity,[60] as found in the present study, denotes that the reaction obeyed the KN criterion and the reaction rates were not influenced by the rates of heat transport. However, the reaction was influenced by mass transport.

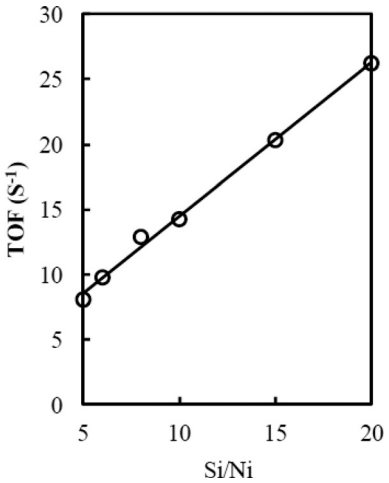

Fig. 10 The Koros–Nowak criterion plot of TOF (S^{-1}) *vs.* Si/Ni for CO_2 methanation using Ni-MCM-41 catalyst at 480 °C.

The XRD of Ni-MCM-41 catalyst after CO_2 methanation was measured, and the peaks assigned to Ni were found, indicating that Ni clusters were formed during the reduction process, but the MCM-41 structure remained and was not damaged. Maybe CO_2 methanation reaction was completely catalyzed by Ni clusters. Another possibility is that the reaction was catalyzed by a metallic cluster together with the incorporated metal located in its vicinity. However, we do not know until now that the reaction was catalyzed mainly by which.

4. Conclusions

Transition metal (M)-incorporated well-ordered mesoporous silica could be obtained by a direct hydrothermal synthesis method from the starting synthesis mixture with a Si/M mole ratio of 5. These transition metal-rich mesoporous silicas are not yet reported. It is found that the chemical bond between transition metal and silicon *via* oxygen was formed as shown by XPS, UV-vis and H_2-TPR analyses, indicating that transition metals were incorporated into a mesoporous silica structure. Ni-MCM-41, Cu-MCM-41 and Co-MCM41 were excellent catalysts for carbon dioxide (CO_2) hydrogenation, although Zn-MCM41 was not. Ni-MCM-41 exhibited excellent catalytic efficiency for CO_2 methanation, giving a reaction rate equation of $r = kC_{CO_2}{}^{0.68}C_{H_2}{}^{3.31}$, while Cu-MCM-41 favored the reverse water gas shift reaction, providing a reaction rate equation of $r = kC_{CO_2}{}^{0.5}C_{H_2}{}^{1.1}$.

Acknowledgements

This research was financially supported by The Environment Research and Technology Development Fund (ERTDF, Ministry of the Environment, Government of Japan, grant no. K123004).

References

1 V. Parvulescu and B.-L. Su, *Catal. Today*, 2001, **69**, 315–323.
2 Y. Yang, S. Lim, G. Du, Y. Chen, D. Ciuparu and G. L. Haller, *J. Phys. Chem. B*, 2005, **109**, 13237–13246.
3 Y. Park, T. Kang, J. Lee, P. Kim, H. Kim and J. Yi, *Catal. Today*, 2004, **97**, 195–203.
4 U. Junges, S. Disser, G. Schmid and F. Schüth, in *Mesoporous Molecular Sieves 1998, Studies in Surface Science and Catalysis*, ed. L. Bonneviot, F. Béland, C. Danumah, S. Giasson and S. Kaliaguine, Elsevier, Amsterdam, 1998, vol. 117, p. 391.
5 T. Linssen, K. Cassiers, P. Cool and E. F. Vansant, *Adv. Colloid Interface Sci.*, 2003, **103**, 121–147.

6 M. Kruk, M. Jaroniec, R. Ryoo and J.-M. Kim, *Microporous Mater.*, 1997, **12**, 93–106.
7 J. F. Bengoa, M. V. Cagnoli, N. G. Gallegos, A. M. Alvarez, L. V. Mogni, M. S. Moreno and S. G. Marchetti, *Microporous Mesoporous Mater.*, 2005, **84**, 153–160.
8 A. Lewandowska, S. Monteverdi, M. Bettahar and M. Ziolek, *J. Mol. Catal. A: Chem.*, 2002, **188**, 85–95.
9 R. Wojcieszak, S. Monteverdi, M. Mercy, I. Nowak, M. Ziolek and M. M. Bettahar, *Appl. Catal., A*, 2002, **268**, 241–253.
10 K. Fang, W. Wei, J. Ren and Y. Sun, *Catal. Lett.*, 2004, **93**(3–4), 235–240.
11 R. B. Biniwale, N. Kariya and M. Ichikawa, *Catal. Lett.*, 2005, **105**(1–2), 83–87.
12 P. Burattin, M. Che and C. Louis, *J. Phys. Chem. B*, 1997, **101**(36), 7060–7074.
13 P. Burattin, M. Che and C. Louis, *J. Phys. Chem. B*, 1999, **103**(30), 6171–6178.
14 P. Burattin, M. Che and C. Louis, *J. Phys. Chem. B*, 1998, **102**(15), 2722–2732.
15 M. Hartman, A. Poeppl and L. Kevan, *J. Phys. Chem.*, 1996, **100**, 9906–9910.
16 Á. Szegedi, M. Popova, V. Mavrodinova, M. Urbán, I. Kiricsi and C. Minchev, *Microporous Mesoporous Mater.*, 2007, **99**, 149–158.
17 G. Du, S. Lim, Y. Yang, C. Wang, L. Pfefferle and G. L. Haller, *J. Catal.*, 2007, **249**, 370–379.
18 D. Liu, R. Lau, A. Borgna and Y. Yang, *Appl. Catal., A*, 2009, **358**, 110–118.
19 W. Stöber and A. Fink, *J. Colloid Interface Sci.*, 1968, **26**, 62–69.
20 C. T. Kresge, M. E. Leonowicz, W. J. J. C. Vartuli and J. S. Beck, *Nature*, 1992, **359**, 710–712.
21 S. M. V. Sivaiah, S. Petit, M. F. Beaufort, D. Eyidi, J. Barrault, C. Batiot-Dupeyrat and S. Valange, *Microporous Mesoporous Mater.*, 2011, **140**, 69–80.
22 S. J. Gregg and K. S.W. Sing, *Adsorption Surface Area and Porosity*, Academic Press, New York, 1982.
23 B.-W. Lu, A. Endo, Y. Inagi and A. Harada, *J. Mater. Sci.*, 2009, **44**, 6463–6469.
24 T. L. Barr, *J. Phys. Chem.*, 1978, **82**, 1801–1810.
25 K. S. Kim and N. Winograd, *Surf. Sci.*, 1974, **43**, 625–643.
26 R. B. Shalvoy, P. J. Reucroft and B. H. Davis, *J. Catal.*, 1979, **56**, 336–348.
27 M. F. Wilson, P. R. Mainwaring, J. R. Brown and J. F. Kriz, *Appl. Catal.*, 1988, **41**, 177–198.
28 P. Dufresene, E. Payen, J. Grimblot and J. P. Bonnelle, *J. Phys. Chem.*, 1981, **85**, 2344–2351.
29 P. Lorenz, J. Finster, G. Wendt, J. V. Salyn, E. K. Zumadilov and V. I. Nefedov, *J. Electron Spectrosc. Relat. Phenom.*, 1979, **16**, 267–276.
30 A. S. Al-Ubaid, *Ind. Eng. Chem. Res.*, 1988, **27**, 790–795.
31 M. L. Occelli, D. Psaras, S. L. Suib and J. M. Stencel, *Appl. Catal.*, 1986, **28**, 143–160.
32 J. C. Vedrine, G. Hollinger and T. M. Duc, *J. Phys. Chem.*, 1978, **82**, 1515–1520.
33 G. Wendt, D. Hentschel, J. Finster, R. Schollner, S. Hanafi and R. S. Mikhail, *J. Chem. Soc., Faraday Trans. 1*, 1983, **79**, 2013–2025.
34 P. Y. Wang, S. Su, J. Xiang, F. Gao, L. S. Sun, S. Hu and S. Y. Lei, *Chem. Eng. J.*, 2013, **225**, 68–75.
35 J. Zhang, S. H. Xu, S. B. Wu and Y. Liu, *Chem. Eng. Sci.*, 2013, **99**, 171–176.
36 W. C. Li, G. T. Du, X. T. Yang, B. Y. Liu, Y. T. Zhang, B. J. Zhao and X. Y. Jiang, *Gaodeng Xuexiao Huaxue Xuebao*, 2004, **25**, 2.
37 Z. H. Ibupoto, N. Jamal, K. Khum, X. Liu and M. Willander, *Sens. Actuators, B*, 2013, **182**, 104–111.
38 A. Galtayries and J. Grimbolt, *J. Electron Spectrosc. Relat. Phenom.*, 1999, **98–99**, 267–275.
39 T. J. Chuang, C. R. Brundle and D. W. Rice, *Surf. Sci.*, 1976, **59**, 413–429.
40 I. G. Casella and M. Guascito, *J. Electroanal. Chem.*, 1999, **476**, 54–63.
41 T. Lehmann, T. Wolff, C. Hamel, P. Veit, B. Garke and A. Seidel-Morgenstern, *Microporous Mesoporous Mater.*, 2012, **151**, 113–125.
42 M. Marciuš, M. Ristic, M. Ivanda and S. Music, *J. Mol. Struct.*, 2013, **1044**, 231–238.
43 B. Scheffer, J. J. Heijeinga and J. A. Moulijn, *J. Phys. Chem.*, 1987, **91**, 4752–4759.
44 C. Lepetit and M. Che, *J. Phys. Chem.*, 1996, **100**, 3137–3143.
45 D. P. Liu, X. Y. Uuek, W. N. E. Cheo, R. Lau, A. Borgna and Y. H. Yang, *J. Catal.*, 2009, **266**, 380–390.
46 X. L. Cheng, H. Zhao, L. H. Huo, S. Gao and J. G. Zhao, *Sens. Actuators, B*, 2004, **102**, 248–252.
47 L. Spanhel and M. A. Anderson, *J. Am. Chem. Soc.*, 1991, **113**, 2826–2833.
48 L. L. Zhang, L. H. Dong, W. J. Yu, L. J. Liu, Y. Deng, B. Liu, H. Q. Wan, F. Gao, K. Q. Sun and L. Dong, *J. Colloid Interface Sci.*, 2011, **355**, 464–471.
49 C. H. He, M. Paulus, W. Chu, J. Find, J. A. Nickl and K. Köhler, *Catal. Today*, 2008, **131**, 305–313.
50 M.-Y. Cheng, C.-J. Pana and B.-J. Hwang, *J. Mater. Chem.*, 2009, **19**, 5193–5120.
51 O. Clause, L. Bonneviot and M. Che, *J. Catal.*, 1992, **138**, 195–205.
52 P. Arnoldy and J. A. Moulijn, *J. Catal.*, 1985, **93**, 38–54.
53 L. Kundakovic and M. Flytzani-Stephanopoulos, *Appl. Catal., A*, 1998, **171**, 13–29.
54 E. Sols, *Collect. Czech. Chem. Commun.*, 1962, **27**, 2621–2627.
55 M. Solc and V. Pour, *Collect. Czech. Chem. Commun.*, 1964, **29**, 857–862.
56 B.-W. Lu and K. Kawamoto, *RSC Adv.*, 2012, **2**, 6800–6805.
57 T. Shido and Y. Iwasawa, *J. Catal.*, 1993, **140**, 575–584.
58 B.-W. Lu and K. Kawamoto, *J. Environ. Chem. Eng.*, 2013, **1**, 300–309.
59 T. Osaki, N. Narita, T. Horiuchi, T. Sugiyama, H. Masuda and K. Suzuki, *J. Mol. Catal. A: Chem.*, 1997, **125**, 63–71.
60 M. Boudart, *AIChE J.*, 1972, **18**, 465–478.
61 R. M. Koros and E. J. Nowak, *Chem. Eng. Sci.*, 1967, **22**, 470.
62 R. J. Madon and M. Boudart, *Ind. Eng. Chem. Fundam.*, 1982, **21**, 438–447.